Adsorption and Reduction from Modified Polypyrrole Enhance Electrokinetic Remediation of Hexavalent Chromium-Contaminated Soil

Jiangyuan Wang
Chongqing University
Qiu Yu
Chongqing University
Yi Zheng
Chongqing University
Jing Li
Chongqing Industry Polytechnic College
Binquan Jiao
Chongqing University
Dongwei Li (litonwei@cqu.edu.cn)
Chongqing University

Research Article

Keywords: Modified polypyrrole, Adsorption, Reutilization, Electrokinetic remediation, Permeable reaction barrier, Cr-contaminated soil

Posted Date: December 15th, 2021

DOI: https://doi.org/10.21203/rs.3.rs-1099895/v1

Version of Record: A version of this preprint was published at Environmental Science and Pollution Research on February 9th, 2022. See the published version at https://doi.org/10.1007/s11356-022-18998-2.

Abstract

Heavy metal pollutant Cr(Ⅵ) in the environment will pose a severe threat to animal and human health. In this work, Fe_3O_4@PPy, Arg@PPy, and Arg/Fe_3O_4@PPy were prepared to enhance adsorption of Cr(Ⅵ) by doping Fe_3O_4 nanoparticles and amino radicals into the original PPy structure. Their characteristics were investigated by FTIR, SEM, EDS, BET analysis, and batch adsorption experiments. And they were used as permeable reaction barriers (PRB) to combine with electrokinetic remediation (EKR) to remediate Cr-contaminated soil. Adsorption experiment results showed that the maximum adsorption capacities of PPy, Fe_3O_4@PPy, Arg@PPy, and Arg/Fe_3O_4@PPy for Cr(Ⅵ) were 60.43 mg/g, 67.12 mg/g, 159.86 mg/g, and 141.50 mg/g, respectively. All of them followed the kinetic pseudo-second-order model and the Langmuir isothermal model with a monolayer adsorption behavior. In EKR/PRB system, the presence of Fe_3O_4@PPy, Arg@PPy, and Arg/Fe_3O_4@PPy obtained the higher Cr(Ⅵ) removal efficiency near the anode than that of the PPy, increasing by 74.60%, 26.04%, 68.64%, respectively. A strong electrostatic attraction between anion contaminants and protonated modified PPy and a reduction from Cr(Ⅵ) to Cr(Ⅲ) appeared in the EKR remediation process under acid conditions. This study opened up a prospect for applying modified PPy composites to treat heavy metal contaminated soil.

1. Introduction

Recent developments in industrialization have heightened the emphasis on soil contamination by heavy metals (Sarwar et al. 2017). The research to date about industrial chromium (Cr) pollution is considered to put an increasing burden on the environment and human health (Wang et al. 2019). That is attributed to its toxicity, persistence, and non-biodegradability gradually accumulating in the environment (Ayangbenro &Babalola 2017). Previously published studies have shown that Cr exists in nature mainly as two stable oxidation states, including hexavalent chromium and trivalent chromium (Sarin &Pant 2006). Cr(Ⅵ) usually occurs as anionic species such as CrO_4^{2-}, $HCrO_4^-$, and $Cr_2O_7^{2-}$, which have high mobility in soil and groundwater, resulting in potential danger of toxicity and carcinogenicity (Eyvazi et al. 2019). Cr(Ⅲ) species, like Cr^{3+}, $Cr_3(OH)_4^{5+}$, and $Cr(OH)^{2+}$, are less toxic and more stable than Cr(Ⅵ) (Sarin &Pant 2006). Therefore, there is an urgent need to find an effective way to address the soil contamination problems caused by Cr.

Numerous methods have been employed to repair Cr-contaminated soil, such as chemical leaching, bioremediation technology, solidification/stabilization, electrokinetic remediation (EKR), etc. (Alidokht et al. 2021, Chen et al. 2021, Sarankumar et al. 2019, Zou et al. 2019). According to the previous literature, EKR, which possesses economic sustainability and satisfies the need to remove various contaminants covering organic pollutants and heavy metals, especially applicable to low permeability soils, is a promising in-situ soil remediation technology (Al-Hamdan &Reddy 2008, Li et al. 2012). Electromigration, electroosmosis, electrophoresis, and electrolysis have been instrumental in our understanding of the mechanism of EKR for heavy metal contaminated soils (Nasiri et al. 2020). However, there are still some limitations of traditional EKR that need to be addressed. For instance, Cr(VI) as the oxygen anion tends to

accumulate in near-anode soil layers and is challenging to remove due to adsorption and potential flattening (Tang et al. 2021, Wen et al. 2021, Yu et al. 2020).

Combined EKR techniques to enhance the Cr(VI) remediation efficiency in near-anode soil layers have got more attention, such as the establishment of a main-auxiliary electrode system, approaching anode electrokinetic method, application of UV radiation and electrokinetic remediation, permeable reactive barrier (PRB) coupled with the electrokinetic process, etc. (Liu et al. 2020, Suzuki et al. 2014, Tang et al. 2021, Wang et al. 2019, Zhang et al. 2012, Zheng et al. 2021). Considerable literature has shown that the EKR/PRB system has the advantage of avoiding secondary contamination of electrolytes (Nasiri et al. 2020, Suzuki et al. 2014, Yeung &Gu 2011). During the EKR/PRB system, the barrier padded with reactive materials bonds with pollutants by reduction, precipitation, and adsorption to remove the anticipated contaminants (Nasiri et al. 2020).

The selection of fillers is central to the entire EKR/PRB, depending on the contaminant category. Active carbon, zeolite, and zero-valent iron are the common reagent medium (Zhou et al. 2021). Previously, a good deal of novel materials with excellent efficiency have been examined. For example, the CaAl-layered double hydroxides were used as a PRB filler for reparation of Cr-contaminated soil in the EKR/PRB system, the union of graphene oxide and fly ash as reaction media could reach a 92.6% removal rate for lead(II) from contaminated soil by EKR/PRB technology (Xu et al. 2016, Zhou et al. 2021). Conductive polymers appear in more studies due to their outstanding electrochemical performance, electrical conductivity, high carrier mobility, and re-utilization (Yuan et al. 2019). Polypyrrole (PPy), which has remarkable environmental stability and non-toxicity as an environmentally friendly polymer material, has recently caught the attention of researchers (Ghorbani et al. 2010, Hasani &Eisazadeh 2013, Hosseini et al. 2015). Under acidic conditions, PPy can protonate and generate electrostatic attraction with anion pollutants (Ting et al. 2021). Moreover, PPy could adsorb anions by carrying nitrogen atoms with positively charged and restore Cr(VI) to Cr(III) (Wei et al. 1993). However, there is a π-π force between the PPy molecular chains, and individual spherical PPy particles are prone to aggregate (Wang et al. 2020). It leads to a small specific surface area limiting their ability to remove Cr(VI) because of low binding sites (Amalraj et al. 2016, Ballav et al. 2014b, Bhaumik et al. 2011). Consequently, it is of great significance to modify PPy to reduce its agglomeration to improve the removal efficiency of Cr(VI).

Recently, Kera et al. have found that adding dopants during polymerization for chain alteration can serve as a suitable means of overcoming the phenomenon of aggregation (Amalraj et al. 2016, Fang et al. 2018, Kera et al. 2016). Furthermore, NH-containing polymers have drawn more attention because of their outstanding chemical reduction ability (Qiu et al. 2014). Based on the research achievement, the adsorptive capacity of modified PPy improves obviously with the number of amino groups within the chemical structure of the dopant (Ballav et al. 2014b, a, Ballav et al. 2012, Bhaumik et al. 2011, Chigondo et al. 2019, Karthik &Meenakshi 2015). They all tend to use modified PPy as an adsorbent to remove pollutants from water, making it possible to remediate contaminated soil with modified PPy as PRB near the anode in the PRB/EKR system.

This study intends to prepare three modified PPy materials, i.e., magnetic PPy (Fe_3O_4@PPy), arginine modified PPy (Arg@PPy), and arginine modified magnetic PPy (Arg/Fe_3O_4@PPy), which are based on PPy by polymerization of pyrrole monomer. The parametric effects on adsorption efficiency, including pH, initial Cr(VI) concentration, dosage, temperature, and contact time, were studied. Kinetics and isotherm studies were performed to research the capacity of adsorption. And then, these composites were used as the PRB fillers near the anode to remediate Cr-contaminated soil. During the EKR/PRB process, electric current, the characteristic of soil and electrolyte, and residual and leaching Cr(VI) content were measured to assess composites' enhancement.

2. Materials And Methods

2.1. Materials and pretreatment

Pyrrole (Py) was obtained from Shanghai Aladdin Biochemical Technology Co., Ltd. Other chemicals like L-Arginine, ammonium persulphate (APS), Fe_3O_4 nanoparticles (50 nm), potassium dichromate ($K_2Cr_2O_7$), of analytical grades, were procured from Chengdu Kelong Chemical Co., Ltd.

The contaminated soil samples in this study were from the 0–20 cm layer of a deserted chromate industrial site located in Chongqing, China. The soil samples were air-dried naturally, and then the apparent impurities and unnecessary debris were removed from them. Next, soil samples were homogenized for the sake of research by grinding in a ball grinder for 12 h and then passing through a 100-mesh sieve.

2.2. Synthesis of composite materials

Three composite materials were prepared as the following procedure by ameliorating other ways (Chigondo et al. 2019).

1. Put 0.3 g of Fe_3O_4 nanoparticles into 80 mL deionized water and then sonicate it for 30 minutes to get an excellent dispersion of Fe_3O_4.
2. Inject 1 mL Py monomer rapidly into the above solution and stir the mixture sharply for about 30 minutes.
3. Put 3.9 g APS into 20 mL deionized water and add it to the 80 mL mixed solution dropwise.
4. Stir the 100 mL mixed solution consecutively for 20 minutes. Place the treated solution at room temperature for 12 h, and add 10 mL acetone to stop the polymerization process.
5. Wash it with deionized water, filter, and vacuum dry them at 60°C for 12 h.
6. Grind the black solid using agate mortar to obtain Fe_3O_4@PPy.

In addition, the preparation of Arg@PPy and Arg/Fe_3O_4@PPy were similar to Fe_3O_4@PPy. The former replaced Fe_3O_4 in the first step with arginine 1.3 g and other steps followed above. The latter was to add 1.3 g of arginine at the start, and the rest of the process was the same as described above.

2.3. Characterization of composite materials and Cr-contaminated soils

Fourier transform infrared spectroscopy (FTIR, Thermo Scientific, USA) analyzed the surface functional groups of the composite materials. The microstructure of the composite materials was investigated using scanning electron microscopy (SEM, Thermo Scientific, USA). Using automated surface area and pore size analysis (MicrotracBEL, Japan) assessed the BET surface area of PPy and its modified materials. The specific analysis results are shown in section 3.1.

An X-ray fluorescence spectrometer (XRF, Thermo Scientific, USA) tested the types and contents of the elements in soil samples. The results are shown in Table 1.

Table 1
Elemental composition of the Cr-contaminated soils

Element	Ratio (%)	Element	Ratio (%)
Si	15.43	Cr	4.74
Ca	14.53	K	1.23
Fe	9.67	S	1.04
Al	7.20	Ti	0.37
Mg	4.70	Na	0.45

2.4. Batch adsorption studies

A series of adsorption studies were conducted in a conical flask of 250 mL and shaken at 200 rpm at room temperature for 24 h (except for the adsorption kinetics experiment). About 50 mg adsorbents were added to 50 mL Cr(Ⅵ) ions solution of 200 mg/L. And the formulas of the adsorption capacity and removal efficiency are given by Eq. (1) and Eq. (2):

$$q=(\frac{C_0-C_t}{m})V \quad (1)$$

$$\eta=\frac{(C_0-C_t)}{C_0}\times 100\% \quad (2)$$

q (mg/g), m (g), and V (L) represent the contaminant's counterbalanced amount per unit mass of adsorbent, the adsorbent mass, and the sample volume, respectively. Where η means removal efficiency, C_0 and C_t are the initial and treated Cr(Ⅵ) concentrations.

Firstly, to understand the significance of new composites, seven different materials, including Fe_3O_4 nanoparticles, arginine alone, conventional powdered activated carbon (AC), pristine PPy, Fe_3O_4@PPy, Arg@PPy, and Arg/Fe_3O_4@PPy, were to compare their adsorption capacities by performing experiments. Secondly, to explore the effect of pH on adsorption properties, 0.1 mol/L HCl and NaOH solutions adjusted pH in the range of 2-12. And then, the subsequent experiments were conducted under optimal pH conditions. Studying the influence of the adsorbent dose was accomplished by changing adsorbents' amounts from 0.01 to 0.09 g. Furthermore, the adsorption kinetics experiment was done by collecting the supernatants from the respective solutions at different times. And adsorption isotherm experiments were performed by varying the initial Cr(VI) concentration from 50 to 400 mg/L. The temperature study was conducted at 298, 308, 318, and 328 K under the same initial Cr(VI) concentration. Finally, in the regeneration experiment, 0.05 mol/L NaOH solution was used to desorb the materials after adsorption (Chigondo et al. 2019). The materials were washed three times with deionized water and dried at 60 ℃. And then repeat the previous operation four times.

2.5. Electrokinetic remediation experiments

The electric repair reactor was made of plexiglass, and it was separated into three areas: anode chamber, sample chamber, and cathode chamber. The soil of the sample room was averagely divided into three sections (S1, S2, S3) from anode to cathode, and a graphite plate and a stainless steel plate were used as the anode and cathode, respectively. An aluminum wire connected a DC power supply to two electrodes at a constant voltage (15 V). In the EKR/PRB, 200 g Cr-contaminated soils were placed in the sample reaction region after pretreatment. 4 g prepared composites were loaded into a 300-mesh filter bag and then put near the anode end. The diagram of the whole installation is shown in Fig. 1. Six groups of control experiments were set up. The initial experimental parameters are shown in Table 2. In the process of EKR, the system current and pH of anode and cathode electrolyte were measured every 12 h. After accomplishing EKR, the feasibility of several materials as PRB fillers was determined by the soil samples' residual and leaching Cr(Ⅵ) concentration.

Table 2
Experimental conditions of EKR

Group	PRB	voltage gradients (V/cm)	Time (d)
EK_1	/	1.5	5
EK_2	AC	1.5	5
EK_3	PPy	1.5	5
EK_4	Fe_3O_4@PPy	1.5	5
EK_5	Arg@PPy	1.5	5
EK_6	Arg/Fe_3O_4@PPy	1.5	5

2.6. Analysis method

The concentration of Cr(Ⅵ) in treated water was determined by the 1,5-Diphenylcarbazide spectrophotometric method. The concentration of Cr(Ⅵ) in contaminated soil was measured based on Chinese standards HJ 1028-2019, using a flame atomic absorption spectrophotometer (AAS, AA6300C, Japan). The leaching toxicity of Cr-contaminated soils was determined, adopting sulfuric acid and nitric acid methods according to Chinese standard HJ/T 299-2007. Moreover, the pH and conductivity of soils were also determined based on potentiometry and electrode method from Chinese standards HJ 962-2018 and HJ 806-2016.

3. Results And Discussion

3.1. Characterization of composite materials

The FTIR spectroscopy of four composites is shown in Fig. 2a. From the chemical structure of pristine PPy, the characteristic peak at 1553 cm^{-1} was assigned to the C=C stretching vibration of the pyrrole ring, which confirmed the successful formation of PPy (Chithra et al. 2018, Sarojini et al. 2021). The other characteristic absorption bands at 1473 cm^{-1}, 1314 cm^{-1}, 1049 cm^{-1}, 902 cm^{-1}, and 682 cm^{-1} corresponded to the C-N stretching of pyrrole ring, C-N in-plane deformation, the plane deformation of =C-H bond, C-H out-of-plane deformation, and C-H out-of-plane ring deformation, respectively (Abdi et al. 2017, Chithra et al. 2018, Sarojini et al. 2021, Wang et al. 2019). On the other hand, the typical characteristics of PPy could also be identified in Fe_3O_4@PPy, Arg@PPy, and Arg/Fe_3O_4@PPy. The FTIR spectrums displayed a slight shift of band, owing to the addition of different dopants. For Fe_3O_4@PPy, Arg@PPy, and Arg/Fe_3O_4@PPy, their bands were shifted to (1557,1473, 1316, 1050, 922 and 685), (1556, 1473, 1315, 1051, 929 and 685), and (1560, 1476, 1299, 1052, 931 and 685), respectively. It indicated that adding dopants caused a subtle displacement compared to the pure PPy bands. That was caused by

both Fe_3O_4 and Arg penetrating the polymer structures to the binding energy of composites affecting each other.

Figure 2b exhibits the N_2 adsorption-desorption isotherms of four composites. The relevant data were estimated to be listed in Table 3. Fe_3O_4@PPy, Arg@PPy, and Arg/Fe_3O_4@PPy revealed a larger surface area and pore volume than pristine PPy. It suggested the success of modified materials with a better adsorption capacity.

Scanning electron microscope analysis was done to investigate the morphology of the composites. SEM images of these polymers were obtained at a magnification of 40000. It can be ascertained from Fig. 2c that pure PPy was composed of stacked and dense spherical particles. And Fe_3O_4@PPy reduced a part of the agglomeration phenomenon compared to PPy. Moreover, the Arg@PPy particles were distinctly smaller than pure PPy particles. Some large particles with smooth surfaces were exposed between those smaller particles, and it is supposed that these smooth and large particles were due to the presence of arginine. However, Arg/Fe_3O_4@PPy particles had a better dispersion because of the adulteration of Fe_3O_4 nanoparticles. As can be seen, the type of dopants impacted the shape and size of polymer particles (Abdi et al. 2017).

EDS spectra are shown in Fig. 2d, revealing the elemental constituents of four materials before EKR. It displayed the obvious peak for Fe, confirming the incorporation of Fe_3O_4 into PPy and Arg@PPy successfully. Furthermore, the semi-quantitative analysis of elements, including C, N, O, Fe and Cr, was carried out through EDS spectra of four materials after EKR. It was found that the weight of Cr is 0.21%, 0.26%, 0.36% and 0.22%, respectively. The results proved the adsorption capacity of the four materials to Cr. And Arg@PPy had the best adsorption ability among them, which matched with SEM and BET analysis results.

Table 3
BET surface area, average pore diameter, and pore volume of PPy, Fe_3O_4@PPy, Arg@PPy, and Arg/Fe_3O_4@PPy

Materials	BET surface area (m^2/g)	Average pore diameter (nm)	Pore volume (cm^3/g)
PPy	6.074	3.283	0.019
Fe_3O_4@PPy	9.463	3.315	0.035
Arg@PPy	12.056	3.289	0.054
Arg/Fe_3O_4@PPy	12.389	3.289	0.060

3.2. Adsorption experiments

3.2.1. Comparison of adsorption properties of different materials

Figure 3 shows the adsorption capacities of seven different materials under the same reaction condition to justify the necessity of the composite materials. From it, the single arginine had little adsorption effect on Cr(Ⅵ) in the solution. And both AC and Fe_3O_4 nanoparticles had a little adsorption capacity. However, the adsorption capacity of polymers was much higher than the above three materials, proving the necessity of materials recombination instead of a simple superposition. Protonation of PPy occurs in the acidic condition, producing electrostatic attraction with Cr(VI) to remove Cr(VI) and reducing probably high-toxicity Cr(VI) to low-toxicity Cr(III) (Shao et al. 2021). The addition of dopant, which causes chain alteration, can reduce the aggregation phenomenon during polymerization, further improving adsorption capacity (Kera et al. 2016).

3.2.2. Effect of pH

The pH of the aqueous solution plays a significant role during the attachment process, which affects adsorbent adsorption on the adsorbate by altering the adsorbent's ionization degree and superficial charge. Cr(Ⅵ) can mainly exist in five forms, namely H_2CrO_4, $HCrO_4^-$, CrO_4^{2-}, $HCr_2O_7^-$, and $Cr_2O_7^{2-}$ (Wang et al. 2012). And the concrete forms of Cr(Ⅵ) are strongly associated with the pH and concentration of the solutions. Under this working concentration, at pH 2 to 6.5, $HCrO_4^-$ is predominant, while CrO_4^{2-} is predominant at pH > 6.5 (Zhao et al. 2010).

The effect of pH (2-12) is shown in Fig. 4a. It offers a downtrend in adsorption property with the increase of pH on the whole. A maximum adsorption capacity was recorded at pH 2 for all the composite materials, consistent with the previous study (Chigondo et al. 2019, Sun et al. 2014). The adsorption capacities of several adsorbents decreased sharply from pH 2 to 3 and then fell further to below 10 mg/g at pH 12. This result at low pH (2-6.5) was mainly attributed to two factors. One was electrostatic adsorption between heavy metal ions and adsorbents due to the protonation of nitrogen atoms included in the adsorbent. So, there was high adsorption to $HCrO_4^-$ by the positively charged surface of composite materials (Avila et al. 2014, Kera et al. 2017, Sun et al. 2014). The other was a possible reduction process, and it was effortless for Cr(Ⅵ) to convert to Cr(Ⅲ) through reduction because of the abundance of electrons in the polymer matrix (Qiu et al. 2014). On the contrary, deprotonation occurred on the positively charged nitrogen atoms of composite materials at relatively high pH, and between CrO_4^{2-} species and materials surface existed electrostatic repulsion. More OH^- in strongly alkaline conditions may compete for binding sites with $CrO4^{2-}$ (Avila et al. 2014, Qiu et al. 2014). In addition, the adsorption capacity of Arg@PPy was significantly higher than that of the other three materials at any pH because per arginine molecule containing four amino groups in Arg@PPy would generate more protonated nitrogen atoms.

3.2.3. Effect of adsorbent dosage

Adsorbent dosage is also a crucial parameter that decides the removal efficiency of Cr(Ⅵ). The effect of adsorbent dosage is observed from Fig. 4b, showing the removal efficiency of four composite materials increased with the increase in adsorbent amount. From 0.01 g to 0.07g, the extent of their growth was

huge because of an increase in binding sites. However, the removal efficiency of Cr(Ⅵ) increased slightly from 0.07 g to 0.09 g. The reason was that the solution's Cr(Ⅵ) ions were limited despite the number of available adsorption sites increasing. Attentionally, the removal efficiency of Cr(Ⅵ) by modified PPy was much higher than that of pristine PPy. Considering the removal efficiency and cost comprehensively, 0.05 g was used to the optimal adsorbent amount for the subsequent experiments.

3.2.4. Effect of the initial Cr(Ⅵ) concentration and temperature

The adsorption of Cr(Ⅵ) by four composite materials was investigated in the initial Cr(Ⅵ) concentration of 50-400 mg/L at four temperatures of 298, 308, 318, and 328 K, shown in Fig. 5. Obviously, the initial Cr(Ⅵ) concentration substantially affected the adsorption capacities of all varieties of composite materials. As a whole, the removal efficiency decreased with an increase in initial Cr(Ⅵ) concentration during this process. Because the adsorbent will reach a saturated state over time. The adsorbent available adsorption sites were relatively more than heavy metal ions at a low initial concentration of Cr(Ⅵ) at a constant dosage. In contrast, at a higher initial Cr(Ⅵ) concentration, the usability of these composites' sites was more petite than heavy metal ions. Hence, there was a descent of Cr(Ⅵ) removal efficiency.

Figure 5a depicts the effect of temperature on Cr(Ⅵ) adsorption by the pristine PPy, demonstrating a faint impact on Cr(Ⅵ) removal efficiency. Fig. 5b, c, and d depict the influence of temperature on the adsorption of Cr(Ⅵ) by Fe_3O_4@PPy, Arg@PPy, and Arg/Fe_3O_4@PPy, respectively. In contrast to Fig. 5a, the Cr(Ⅵ) removal efficiency increased visibly with rising temperature under a constant initial Cr(Ⅵ) concentration, which represented the adsorption of Cr(Ⅵ) on the modified PPy materials was an endothermic process. Especially, it also found that the adsorption property of Arg@PPy was the smallest affected by temperature among the three.

3.2.5. Adsorption isotherm study

Adsorption isotherm is a basic design to investigate the partition of metal ions between the adsorbent and the liquid phase at equilibrium (Chithra et al. 2018). Freundlich adsorption isotherm is appropriate for asymmetrical interface and multimolecular layer adsorption. Langmuir adsorption isotherm abides by the hypothesis of rhythm and uniformity of the adsorbent and combines with unilaminar adsorption onto an interface of numerous blank spots (Sarojini et al. 2021). The linear and nonlinear forms of them, R_L (represents the applicability of the Langmuir isotherm), are shown in Eq. S1-S5. This study shows adsorption isotherms model data fit in Fig. 6.

The result, which included the correlate constants (k_f, n, and q_m) and coefficient (R^2) of adsorption isotherms after fitting, is shown in Table S1. The obtained result showed the highest R^2 value of the linear Langmuir model for the four materials. It suggested that the Langmuir isotherm had a great anastomose with the experimental results compared to other isotherms. On the other hand, based on the obtained experimental data, the R_L at different initial concentrations is illustrated in Table S2. It is evident from the table that the values of R_L were all between 0 and 1. Therefore, the linear Langmuir isotherm was thought

to be favorable for the four materials. Consequently, the conclusion can be drawn that the adsorption mechanisms tended to agree with the Langmuir model.

3.2.6. Adsorption kinetic study

In this study, an adsorption kinetic study was conducted to estimate the adsorption rate of Cr(Ⅵ) with those composites. The obtained experimental results were fitted using pseudo-first-order and pseudo-second-order kinetic models. Those two models assume, respectively, that diffusion and chemisorption are the rate-limiting steps of the adsorption process. The equations of them are shown in Eq. S6-S9.

The graphs associated with the above equation are presented in Fig. 7. The related constants (k_1, k_2, and q) and correlation coefficient (R^2) obtained from Fig. 7 are revealed in Table S3. From Fig. 7, the R^2 obtained through the linear pseudo-second-order kinetic model was the highest among the models. Meanwhile, the adsorption capacities at equilibrium calculated by the pseudo-second-order kinetic model were closer to the values of the experiment. As a result, their adsorption process can be explained by the linear pseudo-second-order kinetic model very well.

3.2.7. Adsorption-desorption study

It is essential to take the adsorbents' cost into account, especially in large-scale applications. So, the reusability of adsorbents is vital. Fig. 8 describes the change in the amount of the materials adsorbed after each desorption. It was noted that the adsorption capacity decreased by degrees as the number of cycles increased for all the adsorbents. For pristine PPy and Fe_3O_4@PPy, the variation range of adsorption capacity was petite. That might be caused by the loss of adsorbents mass during operation. And the loading capacity of Arg@PPy and Arg/Fe_3O_4@PPy reduced relatively larger with the increase in desorption times. But the last adsorption capacity of both was more than 50 percent of the initial capacity, and they account for 52.94% and 55.48% of the initial adsorption capacity, respectively. One reason for this phenomenon was likely to be the imperfect desorption of Cr(Ⅵ) ions (Sarojini et al. 2021). Of course, the loss of mass was another factor.

3.3. Electrokinetic remediation experiment

3.3.1. Variation of electric current

The trend of electric current change in all experiments over time is depicted in Fig. 9a. In EK_1-EK_6, traditional EKR and EKR/PRB systems filled with five different materials were applied.

It is worth mentioning that the initial current of EK_1-EK_6 had a difference. The initial current of EK_4 (3.6 mA), EK_5 (3.0 mA), and EK_6 (4.0 mA) were all higher than that of EK_1 (2.6 mA). However, the initial current of EK_2 (1.7 mA) and EK_3 (1.2 mA) were lower than that of EK_1. The plausible reason for this phenomenon was that modified PPy materials could release more charges at the beginning of the test (Wang et al. 2019). Overall, the electric current increased dramatically to reach a peak in the first 12 h and then a

gradual decline to keep a relative stabilization. The possible reason for this tendency is presented below. The leading cause of the ascending pattern in early times could be the metal ions desorption in the soil (Nasiri et al. 2020). Electrolyte permeated into the contaminated soil, resulting in the movement of Cr(□) diversified forms in the effect of electroosmosis and electromigration (Prakash et al. 2018). It also suggested the migration of toxic and hazardous metals and a positive remediation process. The decrease in electric current afterward could be deemed for reducing mobile free ions in the soil and the formation of hydroxide deposits.

In EK_2, not only did the rate of current increase slowly, but the current was lower than EK_1 from beginning to end. It proved that the presence of AC impeded probably the charge transport to a certain extent. However, the current of EK_3-EK_6 was higher than EK_2. The reason may be the excellent electroconductibility of pristine PPy and modified PPy materials, which favored the charge transportation by the ions in the soil. Thus, the materials of EK_3-EK_6 were more suitable as PRB fillers compared to AC. That further illustrated that fabricated composites as PRB were beneficial to EKR/PRB system.

3.3.2. Variation of pH in electrolyte

As shown in Fig. 9b and c, from beginning to end, the pH of EK_3-EK_6 in the anode compartment was lower than that of EK_1, and it in the cathode compartment was higher than that of EK_1. And it suggested that more H^+ and OH^- were generated because of the current intensity with the presence of PPy or modified PPy materials in the EKR/PRB system. In general, the anolyte pH decreased sharply in EK_1-EK_6 in the early stage of the reaction and then held a strong acid condition until the termination of EKR. Oppositely, the catholyte pH increased at the start of the EK_1-EK_6 tests, and it kept a strong alkali environment until the experiment finished.

Remarkably, as shown in Fig. 9b, the pH value of EK_6 was the lowest at the start. In the first 12 h, the pH value decreased to 2.89 drastically. The strength of the current at the beginning could explain this. And then, it dropped to 2.09 at 72 h, stabilizing around this value until the end of the test subsequently. The low pH of the electrolyte would cause the PRB near the anode chamber to be in an acidic environment, which was beneficial to the adsorbent's adsorption of Cr. Similarly, as shown in Fig. 9c, the cathode chamber pH increased to 11.58 with the first 12 h of the process in EK_6 quickly, and then it kept fluctuating up and down at this value. The presence of Arg/Fe_3O_4@PPy should be responsible for the noticeable phenomenon.

3.3.3. The soil pH and conductivity after EKR

The pH value of contaminated soil in different areas (S1, S2, S3) after EKR is shown in Fig. 10a. The pH value of soil increased gradually from S1 to S3 after EKR in all experiments. The reason was that the electrolysis of water in the anode and cathode produced H^+ and OH^-, and then H^+ and OH^- migrated towards the opposite electrode through the soil, respectively. At the same time, the pH of S1 in EK_3- EK_6

was lower than that of EK_1. As explained in section 3.3.2, PPy and modified PPy materials were possibly beneficial to the generation of H^+.

The conductivity of contaminated soil in different areas before and after EKR is shown in Fig. 10b. The conductivity of S1 was generally higher than that of S3 after EKR. It could be attributed to more enrichment of free anions near the anode than free cations near the cathode because the cathode cations combined with OH^- to form hydroxide precipitation. Moreover, the conductivity of S1 in EK_3-EK_6 was much higher than that of the initial. Maybe because PPy has good charge storage capacity and good electrochemical performance, it could release charge to maintain high conductivity nearby (Wang et al. 2019). As for the conductivity difference among EK_3-EK_6, the type of the dopant was the primary reason. They affected the conductivity of the polymers by altering their arrangement and aggregation of molecular chains. From Fig. 10b, Fe_3O_4 nanoparticles were the most conducive to the improvement of conductivity.

3.3.4. Residual and leaching concentration of Cr(Ⅵ)

The residual Cr(Ⅵ) concentration was an essential criterion for measuring the effect of EKR. Cr(Ⅵ) concentration in soil was 212.693 mg/kg before EKR. As shown in Fig. 10c, it demonstrated two different patterns of change. The first one was a stepped distribution from S3 to S1 in EK_1-EK_3 and EK_5. That resulted from the directional migration of Cr(Ⅵ) in the form of anions from the cathode to the anode in the EKR system. And the contaminants near the anode accumulated continually during the migration process, leading to the phenomenon of aggregation. The other was in EK_4 and EK_6, which resembled a normal distribution high in the middle and low on the two sides. The concentration of S1 was lower than that of the former, which was significantly different from the previous model. The existence of Fe_3O_4@PPy and Arg/Fe_3O_4@PPy could be reasonable for explaining this phenomenon. The electrostatic attraction between the positively charged nitrogen atoms and the negatively charged Cr(Ⅵ) ions led to the PPy adsorption to Cr(Ⅵ) species. Then perhaps the Cr(Ⅵ) on the PPy interface occurred reduction reaction on account of electron-rich polymeric moieties of PPy to become Cr(Ⅲ) (Wang et al. 2019).

Additionally, the biggest otherness of Fe_3O_4@PPy and Arg/Fe_3O_4@PPy with other materials was that they contained Fe_3O_4 nanoparticles. As shown in Fig. 11, the concentration of Fe in the anolyte reached a peak at 24 h and then declined until the EKR process was over. It could be speculated that Fe_3O_4 under a complex background would be released from the composite materials by Eq. (3). And Fe^{2+} near the anode would reduce Cr(Ⅵ) to Cr(Ⅲ), further improving the Cr(Ⅵ) removal efficiency in S1. The lowest Cr(Ⅵ) concentration was found in section S1 of EK_4. It illustrated the importance of Fe_3O_4@PPy for the removal of Cr(Ⅵ) in the EKR system. Unlike the consequence in section 3.2.1., the effect of Fe_3O_4@PPy was better than that of Arg/Fe_3O_4@PPy in the soil, possibly because it was in a more complex environment without pH 2. But the Cr(Ⅵ) removal efficiency in S1 of EK_5 still increased by 26.04% compared to EK_3, illustrating that the profound of Arg@PPy for EKR was superior to pure PPy.

$Fe_3O_4+8H^+ \rightarrow Fe^{2+}+2Fe^{3+}+4H_2O$ (3)

Unreasonable disposal of Cr-contaminated soil will cause substantial environmental hazards, and leaching toxicity was an essential indicator for identifying hazardous waste. Therefore, it was necessary to reduce the leaching concentration of Cr(Ⅵ) in Cr-contaminated soil. Cr(Ⅵ) initial leaching concentration was 8.412 mg/L. The pattern of the Cr(Ⅵ) leaching concentration after EKR was similar to the corresponding Cr(Ⅵ) residual concentration in soil. As shown in Fig. 10d, the lower the leaching concentration was meant to the higher the removal efficiency. That was the reason why its tendency was consistent with Fig. 10c.

4. Conclusion

The adsorption property of Arg@PPy and Arg/Fe_3O_4@PPy was much higher than pristine PPy in Cr-polluted water at pH 2. PPy, Fe_3O_4@PPy, Arg@PPy, and Arg/Fe_3O_4@PPy accorded well with the kinetic pseudo-second-order and Langmuir isothermal models. In the EKR/PRB system, the three composites (Fe_3O_4@PPy, Arg@PPy, and Arg/Fe_3O_4@PPy) would influence system current, soil characteristic, and electrolyte pH, which was beneficial to improve the removal efficiency of Cr(Ⅵ), especially near the anode. The removal process of Cr(Ⅵ) by them included electrostatic attraction between Cr(Ⅵ) and protonated PPy and a possible reduction process from high-toxicity Cr(Ⅵ) to low-toxicity Cr(Ⅲ). All in all, this study offered a few ideas to deal with Cr-contaminated soil and water using green adsorbents.

Declarations

Acknowledgments This research did not receive any specific grant from funding agencies in the public, commercial, or not-for-profit sectors.

Ethical Approval Not applicable

Consent to Participate Yes

Consent to Publish Yes

Authors Contributions All authors contributed to the study conception and design. Jiangyuan Wang, Qiu Yu, Yi Zheng, and Jing Li performed material preparation, data collection, and analysis. The first draft of the manuscript was written by Jiangyuan Wang. Binquan Jiao and Dongwei Li performed supervision and conceptualization. And all authors commented on previous versions of the manuscript and approved the final manuscript.

Conflicts of interest There are no conflicts to declare.

Funding No

Availability of data and materials All data generated or analyzed during this study are included in this published article. And all data are fully available without restriction.

References

1. Abdi S, Nasiri M, Mesbahi A, Khani MH (2017): Investigation of uranium (VI) adsorption by polypyrrole. J Hazard Mater 332, 132-139
2. Al-Hamdan AZ, Reddy KR (2008): Transient behavior of heavy metals in soils during electrokinetic remediation. Chemosphere 71, 860-71
3. Alidokht L, Oustan S, Khataee A, Neyshaburi MR, Reyhanitabar A (2021): Stabilization of chromium(VI) by hydroxysulfate green rust in chromium(VI)-contaminated soils. Pedosphere 31, 645-657
4. Amalraj A, Selvi MK, Rajeswari A, Pius A (2016): Preparation and characterization of aspartic acid doped polypyrrole for the efficient removal of Cr(VI) from aqueous solution. Journal of Water Process Engineering 11, 162-173
5. Avila M, Burks T, Akhtar F, Göthelid M, Lansåker PC, Toprak MS, Muhammed M, Uheida A (2014): Surface functionalized nanofibers for the removal of chromium(VI) from aqueous solutions. Chem Eng J 245, 201-209
6. Ayangbenro AS, Babalola OO (2017): A New Strategy for Heavy Metal Polluted Environments: A Review of Microbial Biosorbents. Int J Environ Res Public Health 14
7. Ballav N, Maity A, Mishra SB (2012): High efficient removal of chromium(VI) using glycine doped polypyrrole adsorbent from aqueous solution. Chem Eng J 198, 536-546
8. Ballav N, Choi HJ, Mishra SB, Maity A (2014a): Synthesis, characterization of Fe3O4@glycine doped polypyrrole magnetic nanocomposites and their potential performance to remove toxic Cr(VI). J Ind Eng Chem 20, 4085-4093
9. Ballav N, Choi HJ, Mishra SB, Maity A (2014b): Polypyrrole-coated halloysite nanotube clay nanocomposite: Synthesis, characterization and Cr(VI) adsorption behaviour. Applied Clay Science 102, 60-70
10. Bhaumik M, Maity A, Srinivasu VV, Onyango MS (2011): Enhanced removal of Cr(VI) from aqueous solution using polypyrrole/Fe3O4 magnetic nanocomposite. J Hazard Mater 190, 381-390
11. Chen Y, Wu H, Sun P, Liu J, Qiao S, Zhang D, Zhang Z (2021): Remediation of Chromium-Contaminated Soil Based on Bacillus cereus WHX-1 Immobilized on Biochar: Cr(VI) Transformation and Functional Microbial Enrichment. Front Microbiol 12, 641913
12. Chigondo M, Paumo HK, Bhaumik M, Pillay K, Maity A (2019): Magnetic arginine-functionalized polypyrrole with improved and selective chromium(VI) ions removal from water. Journal of Molecular Liquids 275, 778-791
13. Chithra K, Akshayaraj RT, Pandian K (2018): Polypyrrole-Protected Magnetic Nanoparticles as an Excellent Sorbent for Effective Removal of Cr(VI) and Ni(II) from Effluent Water: Kinetic Studies and

Error Analysis. Arabian Journal for Science and Engineering 43, 6219-6228

14. Eyvazi B, Jamshidi-Zanjani A, Khodadadi Darban A (2019): Immobilization of hexavalent chromium in contaminated soil using nano-magnetic MnFe2O4. J Hazard Mater 365, 813-819
15. Fang W, Jiang X, Luo H, Geng J (2018): Synthesis of graphene/SiO2@polypyrrole nanocomposites and their application for Cr(VI) removal in aqueous solution. Chemosphere 197, 594-602
16. Ghorbani M, Esfandian H, Taghipour N, Katal R (2010): Application of polyaniline and polypyrrole composites for paper mill wastewater treatment. Desalination 263, 279-284
17. Hasani T, Eisazadeh H (2013): Removal of Cd (II) by using polypyrrole and its nanocomposites. Synthetic Metals 175, 15-20
18. Hosseini S, Ekramul Mahmud NHM, Binti Yahya R, Ibrahim F, Djordjevic I (2015): Polypyrrole conducting polymer and its application in removal of copper ions from aqueous solution. Materials Letters 149, 77-80
19. Karthik R, Meenakshi S (2015): Removal of hexavalent chromium ions from aqueous solution using chitosan/polypyrrole composite. Desalin Water Treat 56, 1587-1600
20. Kera NH, Bhaumik M, Ballav N, Pillay K, Ray SS, Maity A (2016): Selective removal of Cr(VI) from aqueous solution by polypyrrole/2,5-diaminobenzene sulfonic acid composite. J Colloid Interface Sci 476, 144-157
21. Kera NH, Bhaumik M, Pillay K, Ray SS, Maity A (2017): Selective removal of toxic Cr(VI) from aqueous solution by adsorption combined with reduction at a magnetic nanocomposite surface. J Colloid Interface Sci 503, 214-228
22. Li D, Xiong Z, Nie Y, Niu Y-Y, Wang L, Liu Y-Y (2012): Near-anode focusing phenomenon caused by the high anolyte concentration in the electrokinetic remediation of chromium(VI)-contaminated soil. J Hazard Mater 229-230, 282-291
23. Liu YX, Ke X, Wu XY, Ke CJ, Chen RY, Chen X, Zheng X, Jin YC, Van der Bruggen B (2020): Simultaneous Removal of Trivalent Chromium and Hexavalent Chromium from Soil Using a Modified Bipolar Membrane Electrodialysis System. Environmental Science & Technology 54, 13304-13313
24. Nasiri A, Jamshidi-Zanjani A, Khodadadi Darban A (2020): Application of enhanced electrokinetic approach to remediate Cr-contaminated soil: Effect of chelating agents and permeable reactive barrier. Environ Pollut 266, 115197
25. Prakash P, Chakraborty PK, Priya T, Mishra BK (2018): Performance evaluation of saponin over other organic acid and tap water for removal of chromium in tannery sludge by electrokinetic enhancement. Separation Science and Technology 54, 173-182
26. Qiu B, Xu CX, Sun DZ, Yi H, Guo J, Zhang X, Qu HL, Guerrero M, Wang XF, Noel N, Luo ZP, Guo ZH, Wei SY (2014): Polyaniline Coated Ethyl Cellulose with Improved Hexavalent Chromium Removal. Acs Sustainable Chemistry & Engineering 2, 2070-2080
27. Sarankumar RK, Selvi A, Murugan K, Rajasekar A (2019): Electrokinetic (EK) and Bio-electrokinetic (BEK) Remediation of Hexavalent Chromium in Contaminated Soil Using Alkalophilic Bio-anolyte. Indian Geotechnical Journal 50, 330-338

28. Sarin V, Pant KK (2006): Removal of chromium from industrial waste by using eucalyptus bark. Bioresour Technol 97, 15-20
29. Sarojini G, Venkateshbabu S, Rajasimman M (2021): Facile synthesis and characterization of polypyrrole - iron oxide - seaweed (PPy-Fe3O4-SW) nanocomposite and its exploration for adsorptive removal of Pb(II) from heavy metal bearing water. Chemosphere 278, 130400
30. Sarwar N, Imran M, Shaheen MR, Ishaque W, Kamran MA, Matloob A, Rehim A, Hussain S (2017): Phytoremediation strategies for soils contaminated with heavy metals: Modifications and future perspectives. Chemosphere 171, 710-721
31. Shao Y, Fan Z, Zhong M, Xu W, He C, Zhang Z (2021): Polypyrrole/bacterial cellulose nanofiber composites for hexavalent chromium removal. Cellulose 28, 2229-2240
32. Sun X, Yang L, Xing H, Zhao J, Li X, Huang Y, Liu H (2014): High capacity adsorption of Cr(VI) from aqueous solution using polyethylenimine-functionalized poly(glycidyl methacrylate) microspheres. Colloids and Surfaces A: Physicochemical and Engineering Aspects 457, 160-168
33. Suzuki T, Kawai K, Moribe M, Niinae M (2014): Recovery of Cr as Cr(III) from Cr(VI)-contaminated kaolinite clay by electrokinetics coupled with a permeable reactive barrier. J Hazard Mater 278, 297-303
34. Tang J, Qiu Z, Tang H, Wang H, Sima W, Liang C, Liao Y, Li Z, Wan S, Dong J (2021): Coupled with EDDS and approaching anode technique enhanced electrokinetic remediation removal heavy metal from sludge. Environ Pollut 272, 115975
35. Ting MS, Narasimhan BN, Travas-Sejdic J, Malmström J (2021): Soft conducting polymer polypyrrole actuation based on poly(N-isopropylacrylamide) hydrogels. Sensors and Actuators B: Chemical 343
36. Wang Q, Guan Y, Liu X, Ren X, Yang M (2012): High-capacity adsorption of hexavalent chromium from aqueous solution using magnetic microspheres by surface dendrimer graft modification. J Colloid Interface Sci 375, 160-6
37. Wang Y, Huang L, Wang Z, Wang L, Han Y, Liu X, Ma T (2019): Application of Polypyrrole flexible electrode for electrokinetic remediation of Cr(VI)-contaminated soil in a main-auxiliary electrode system. Chem Eng J 373, 131-139
38. Wang Y, Yin Q, Du K, Mo S, Yin Q (2020): Thermoelectric Properties of Polypyrrole Nanotubes. Macromolecular Research 28, 973-978
39. Wei C, German S, Basak S, Rajeshwar K (1993): Reduction of Hexavalent Chromium in Aqueous-Solutions by Polypyrrole. Journal of the Electrochemical Society 140, L60-L62
40. Wen DD, Guo XP, Fu RB (2021): Inhibition characteristics of the electrokinetic removal of inorganic contaminants from soil due to evolution of the acidic and alkaline fronts. Process Saf Environ 155
41. Xu YF, Xu XJ, Hou HT, Zhang J, Zhang DY, Qian GR (2016): Moisture content-affected electrokinetic remediation of Cr(VI)-contaminated clay by a hydrocalumite barrier. Environmental Science and Pollution Research 23, 6517-6523

42. Yeung AT, Gu YY (2011): A review on techniques to enhance electrochemical remediation of contaminated soils. J Hazard Mater 195, 11-29
43. Yu Q, Yan Y, Lin H, Li H, Zheng Y, Jiao B, Yu L, Li D (2020): Biosurfactants enhanced electrokinetic treatment of Cr from chromite ore processing residue based on chemical fractions. Journal of Water Process Engineering 36
44. Yuan X, Floresyona D, Aubert P-H, Bui T-T, Remita S, Ghosh S, Brisset F, Goubard F, Remita H (2019): Photocatalytic degradation of organic pollutant with polypyrrole nanostructures under UV and visible light. Applied Catalysis B: Environmental 242, 284-292
45. Zhang J, Xu YF, Li WT, Zhou JZ, Zhao J, Qian GG, Xu ZP (2012): Enhanced remediation of Cr(VI)-contaminated soil by incorporating a calcined-hydrotalcite-based permeable reactive barrier with electrokinetics. J Hazard Mater 239, 128-134
46. Zhao Y-G, Shen H-Y, Pan S-D, Hu M-Q, Xia Q-H (2010): Preparation and characterization of amino-functionalized nano-Fe3O4 magnetic polymer adsorbents for removal of chromium(VI) ions. Journal of Materials Science 45, 5291-5301
47. Zheng Y, Li H, Yu Q, Yu L, Jiao B, Li D (2021): Application of UV radiation for in-situ Cr(VI) reduction from contaminated soil with electrokinetic remediation. J Hazard Mater 416, 125806
48. Zhou H, Liu Z, Li X, Xu J (2021): Remediation of lead (II)-contaminated soil using electrokinetics assisted by permeable reactive barrier with different filling materials. J Hazard Mater 408, 124885
49. Zou Q, Gao Y, Yi S, Jiang J, Aihemaiti A, Li D, Yang M (2019): Multi-step column leaching using low-molecular-weight organic acids for remediating vanadium- and chromium-contaminated soil. Environ Sci Pollut Res Int 26, 15406-15413

Figures

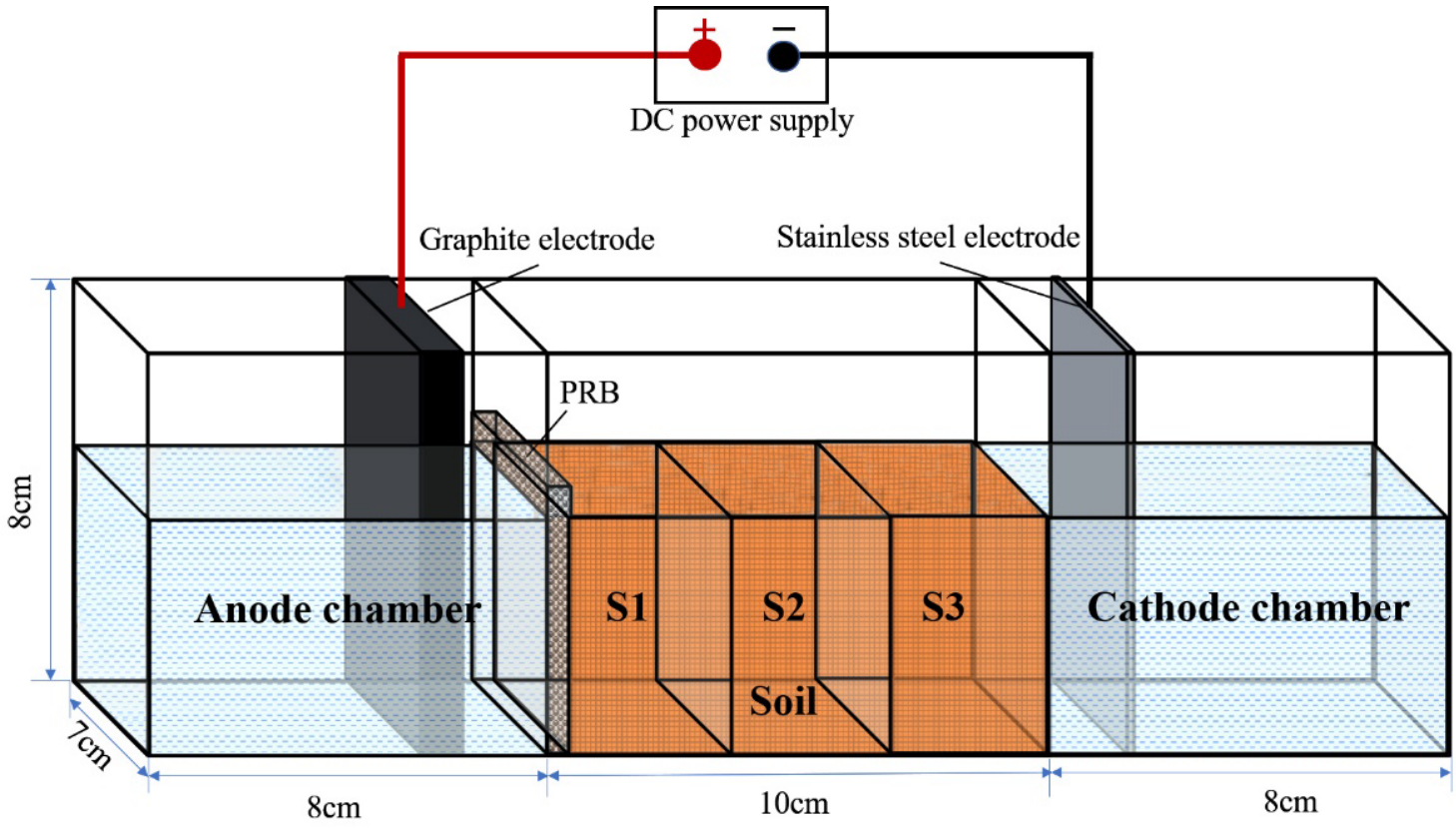

Figure 1

The installation diagram of EKR/PRB

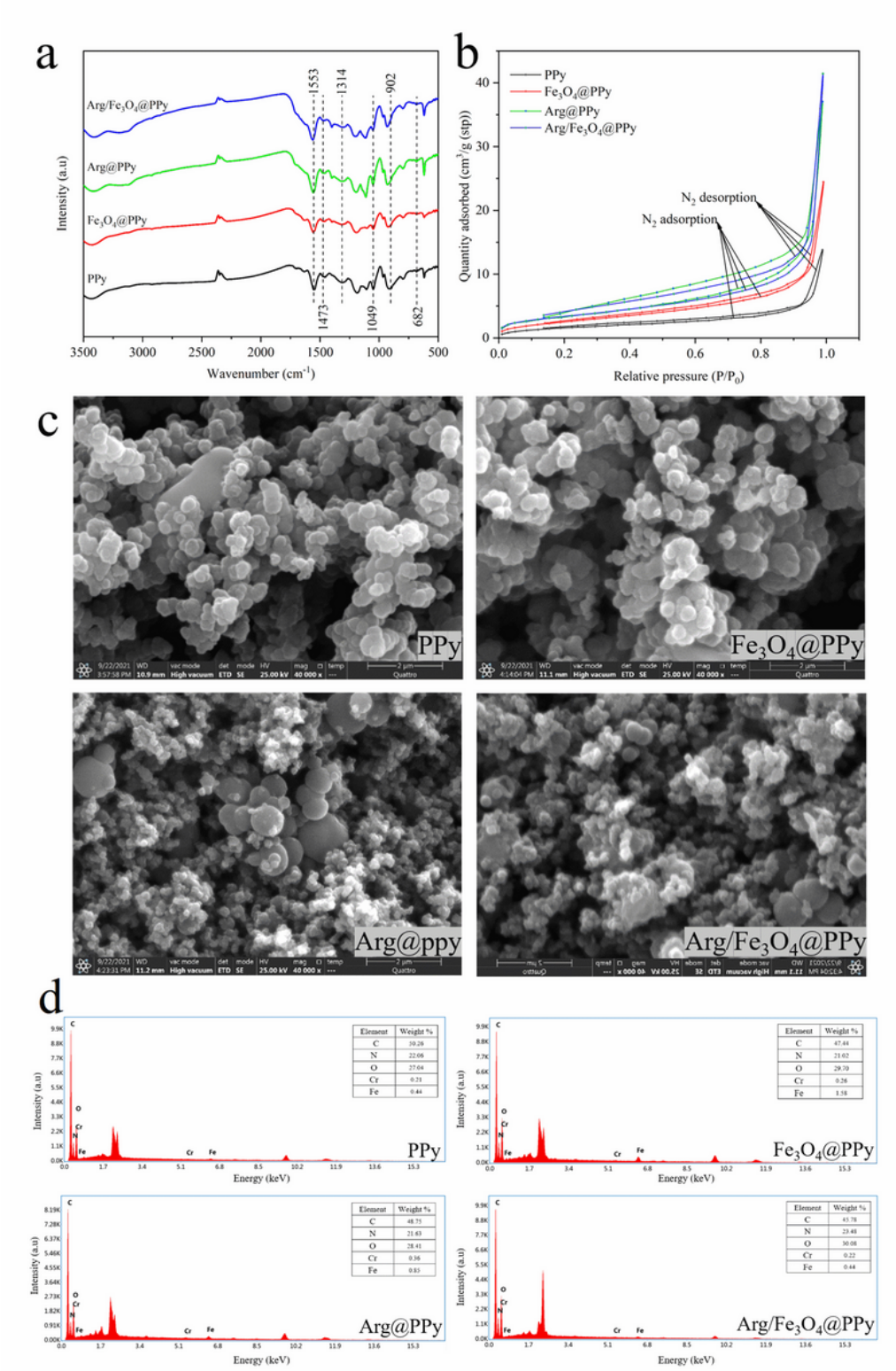

Figure 2

(a) FTIR (b) N2 adsorption-desorption isotherm (c) SEM (d) EDS photograph of four composites

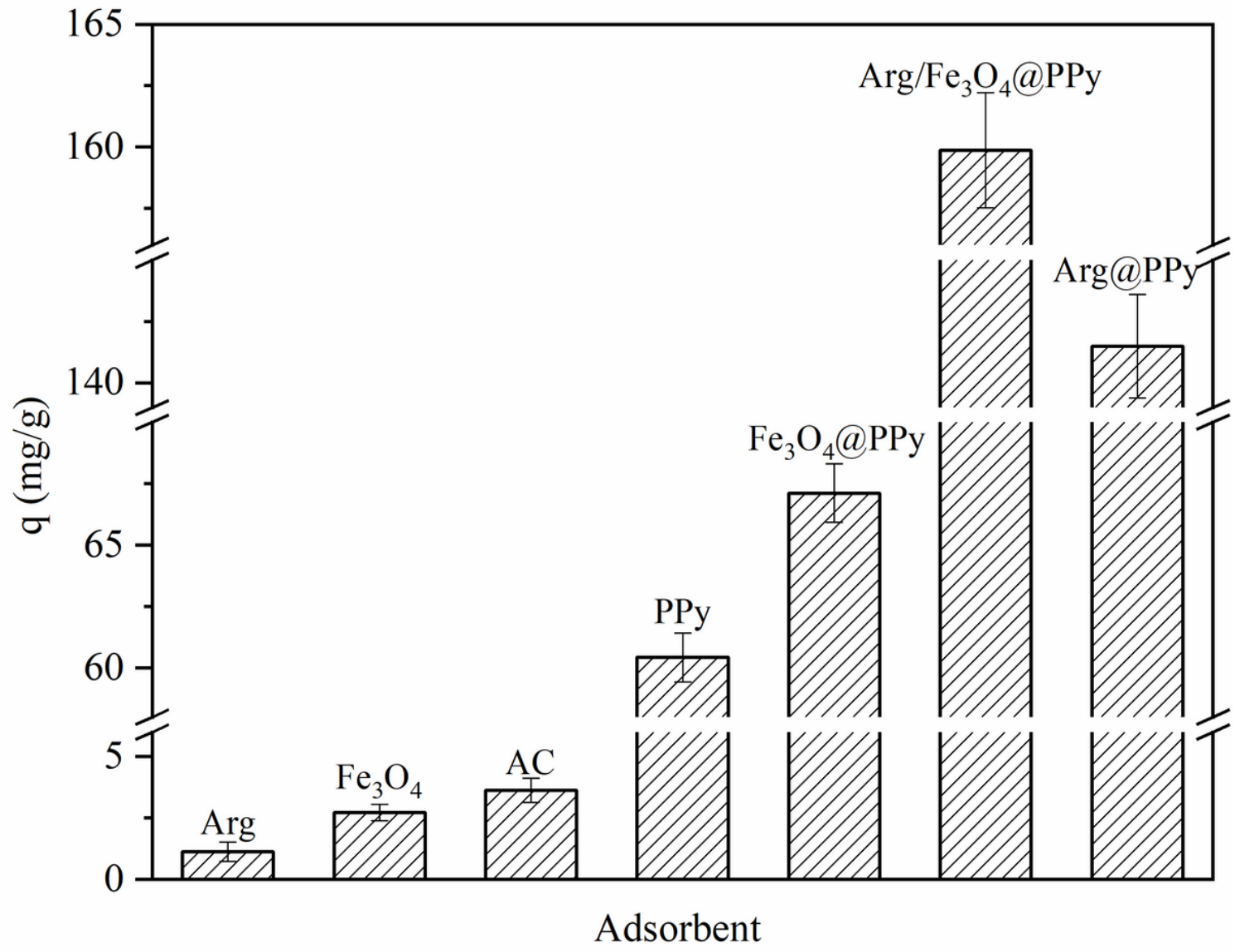

Figure 3

The adsorption capacities of seven different materials

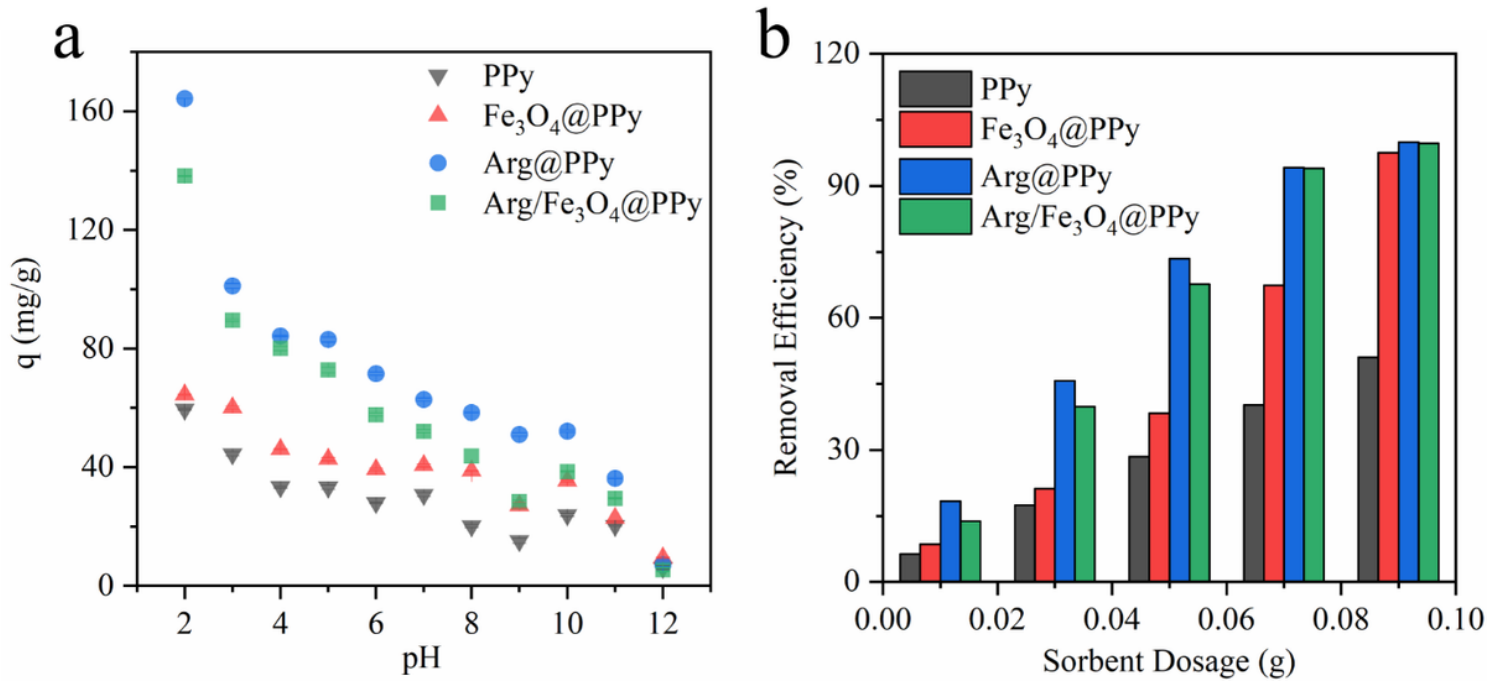

Figure 4

(a) Effect of pH on adsorption capacity (b) Effect of sorbent dosage on Cr(Ⅵ) removal efficiency

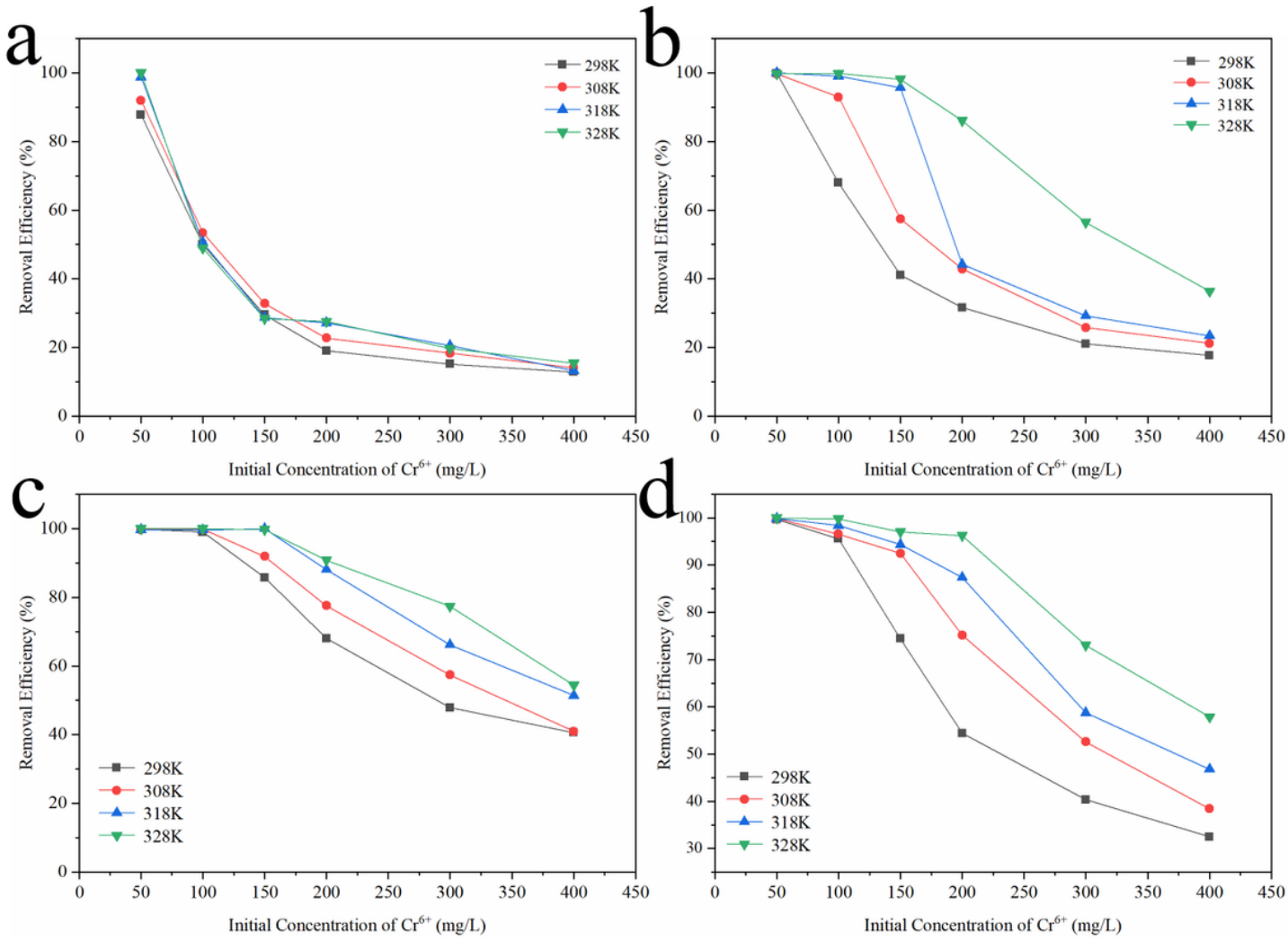

Figure 5

Effect of temperature and initial Cr(Ⅵ) concentration on the removal efficiency of Cr(Ⅵ) by (a) PPy, (b) Fe3O4@PPy, (c) Arg@PPy, and (d) Arg/Fe3O4@PPy

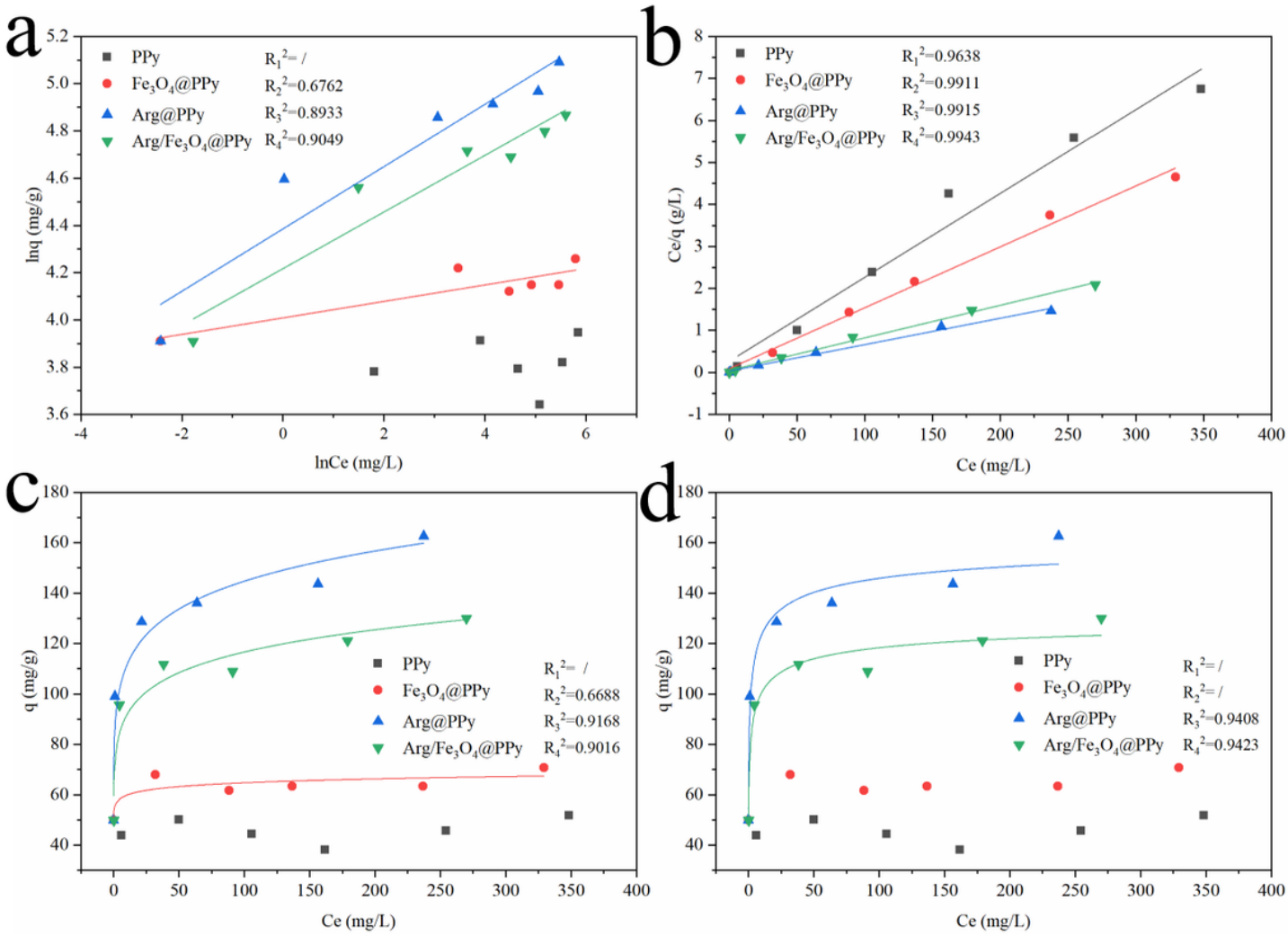

Figure 6

Adsorption isotherms for Cr(Ⅵ) ions removal by four composites and fit data to linear (a) Freundlich, (b) Langmuir, nonlinear (c) Freundlich, and (d) Langmuir adsorption isotherms model data fit

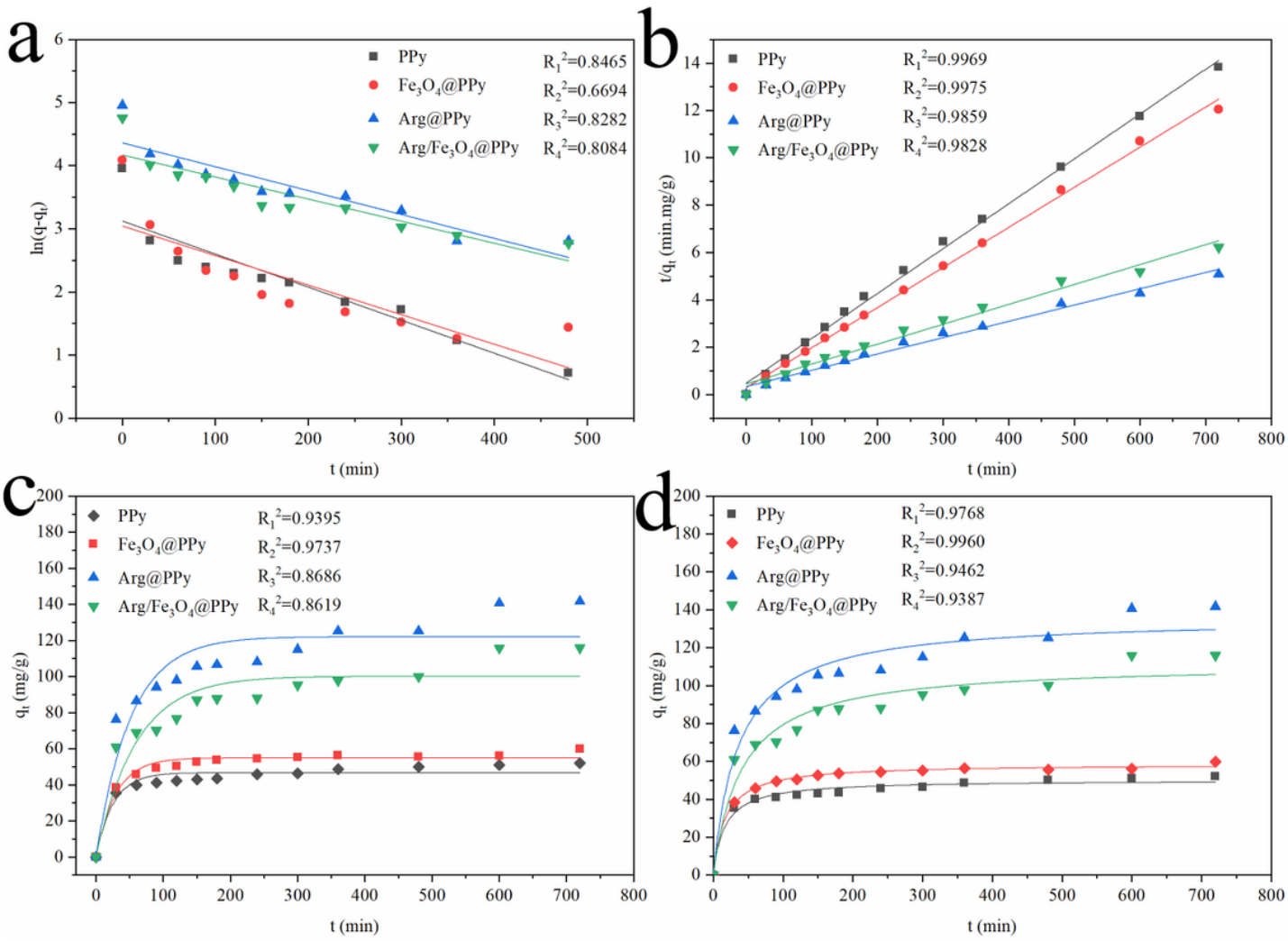

Figure 7

Adsorption kinetics for Cr(Ⅵ) ions removal by four composites and fit data to linear (a) pseudo-first-order, (b) pseudo-second-order, nonlinear (c) pseudo-first-order, and (d) pseudo-second-order kinetic models data fit

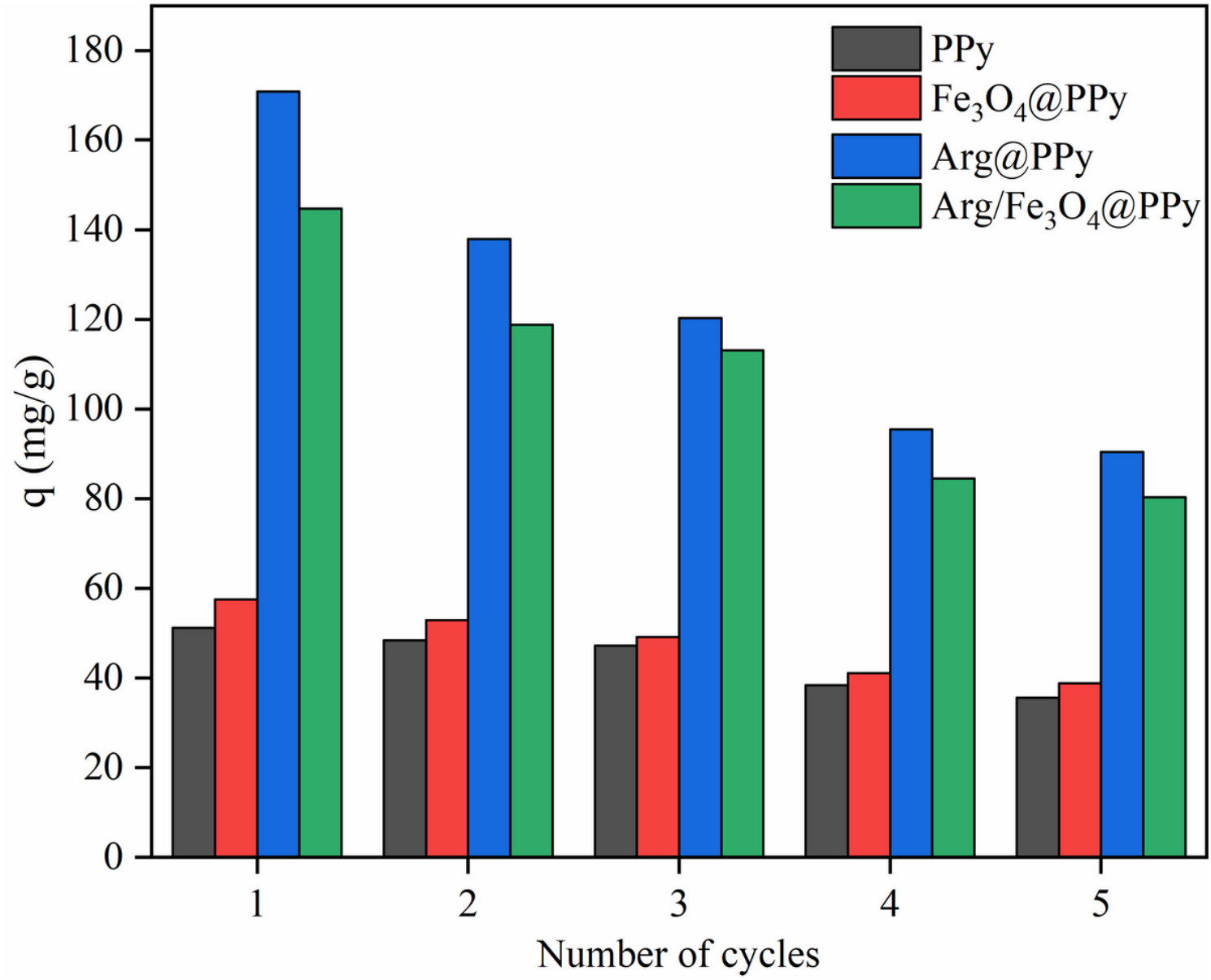

Figure 8

Effect of the number of cycles on adsorption of Cr(Ⅵ) ions by four materials

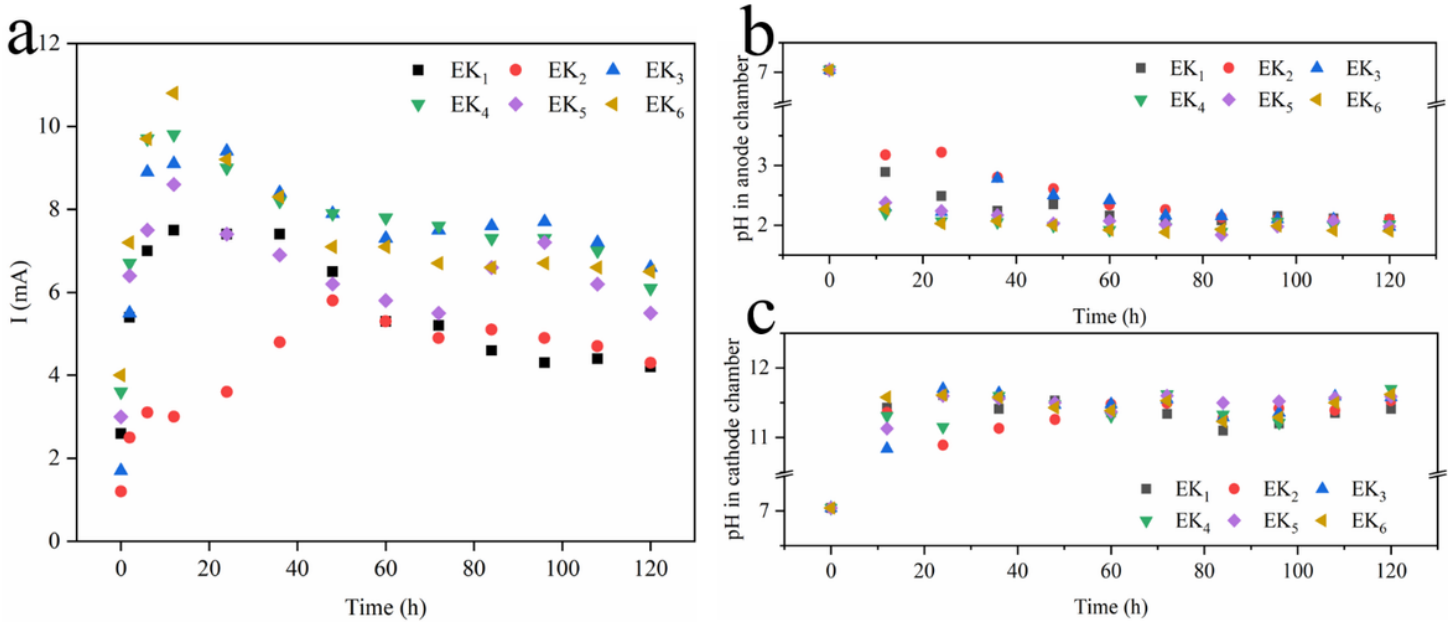

Figure 9

The variation of (a) electric current in the EKR system and pH (b) in the anode and (c) cathode chambers over time

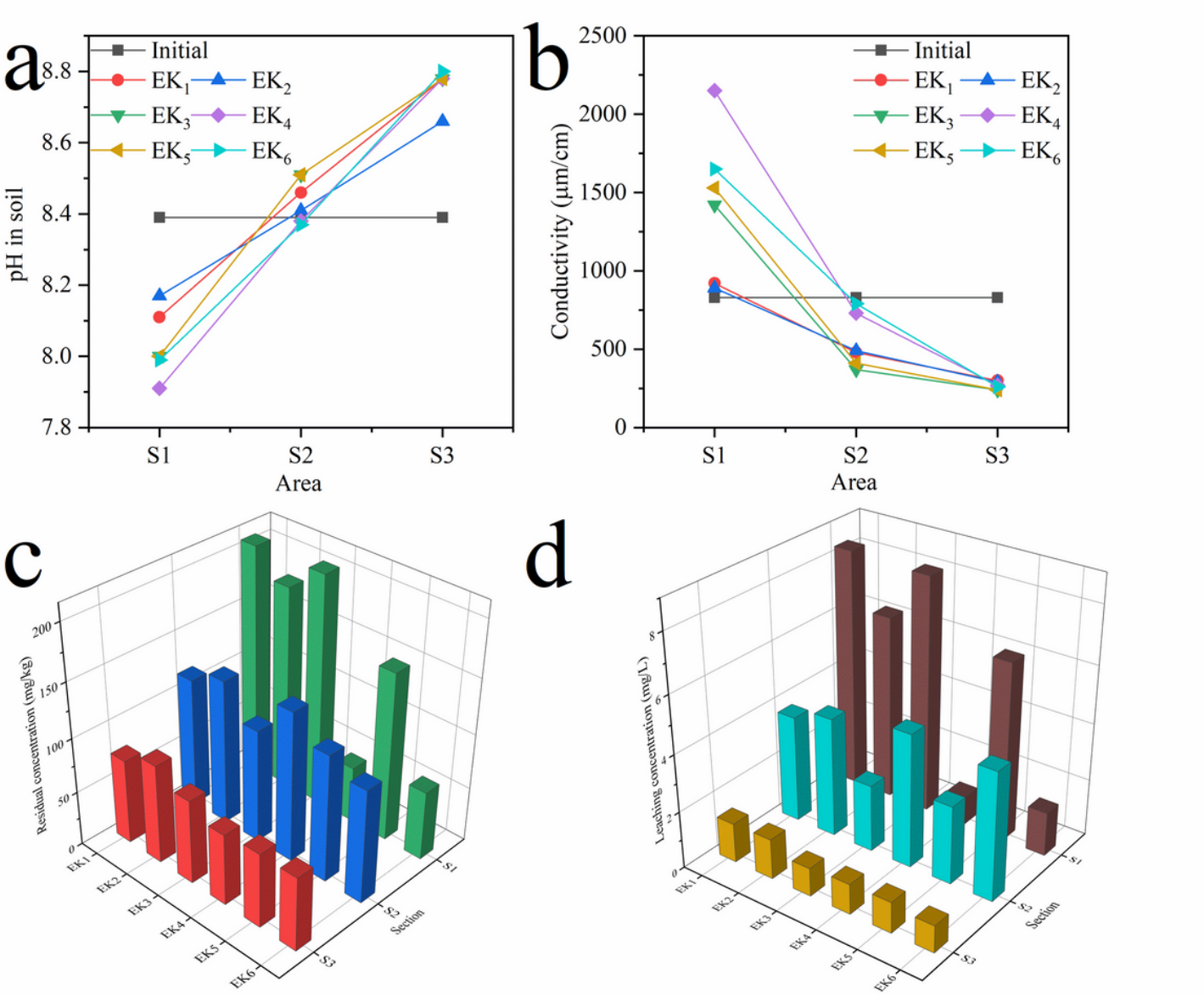

Figure 10

The soil (a) pH, (b) conductivity, (c) residual Cr(Ⅵ) concentration, and (d) leaching Cr(Ⅵ) concentration after EKR

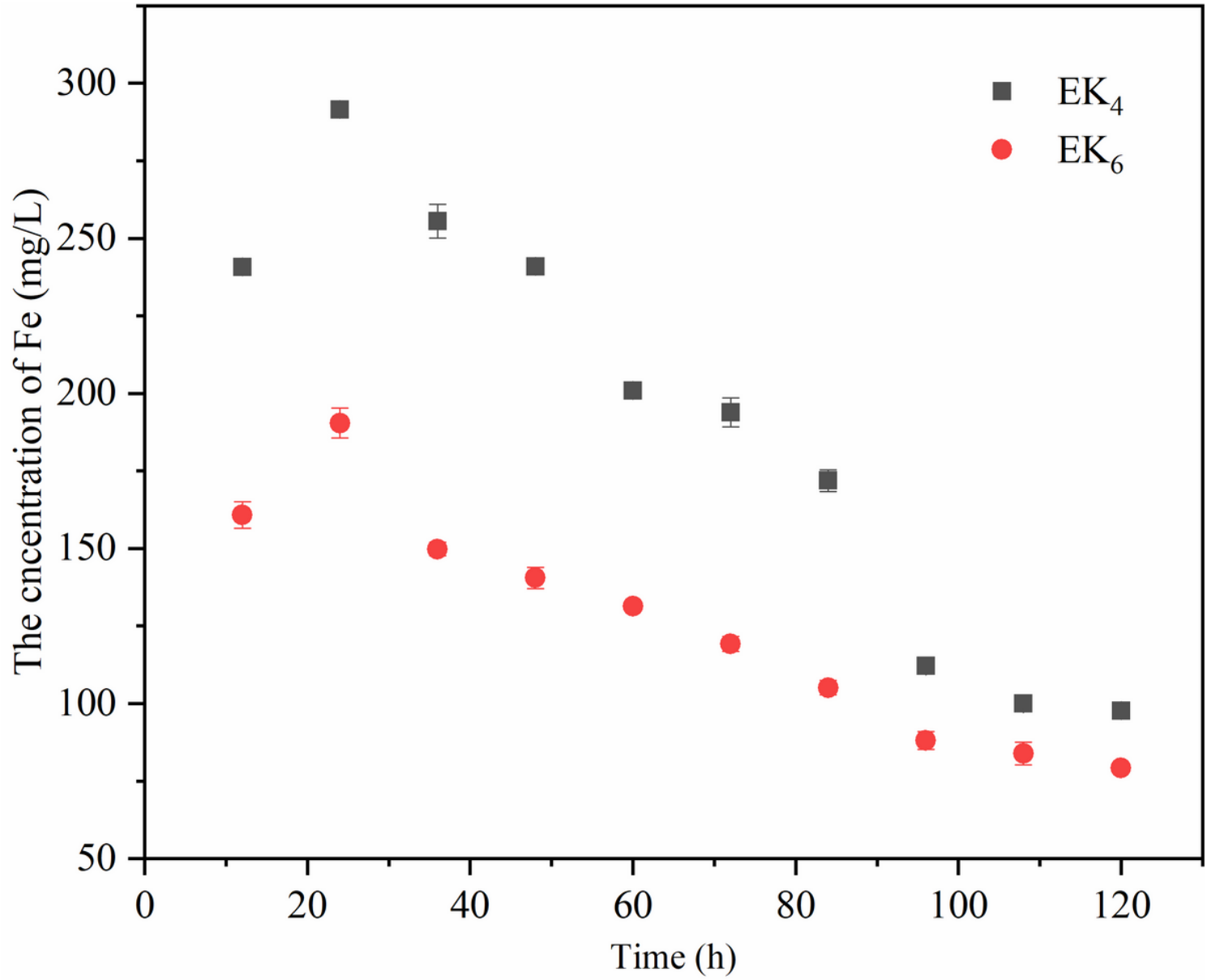

Figure 11

The variation of Fe concentration in the anolyte over time

Supplementary Files

This is a list of supplementary files associated with this preprint. Click to download.

- supplementaryinformation.docx